Energy release rate of fiber/matrix interface crack growth in cross-ply laminates under transverse loading: effect of the 0°/90° interface and of 0° layer thickness

Luca Di Stasio[a,b], Janis Varna[a], Zoubir Ayadi[b]

[a]*Luleå University of Technology, University Campus, SE-97187 Luleå, Sweden*
[b]*Université de Lorraine, EEIGM, IJL, 6 Rue Bastien Lepage, F-54010 Nancy, France*

Abstract

Models of Representative Volume Elements (RVEs) of cross-ply laminates with different geometric configurations and damage states are studied. Debond growth is characterized by the estimation of the Mode I and Mode II Energy Release Rate (ERR) using the Virtual Crack Closure Technique (VCCT). It is found that the presence of the 0°/90° interface and the thickness of the 0° layer have no effect, apart from laminates with *ultra-thin* 90° plies where it is however modest. The present analysis support the claim that debond growth is not affected by the ply-thickness effect.

Keywords: Polymer-matrix Composites (PMCs), Fibre/matrix bond, Debonding, Finite Element Analysis (FEA)

1. Introduction

Since the development of the *spread tow* technology or "FUKUI method" [1], significant efforts have been directed toward the characterization of *thin-ply* laminates [2, 3, 4, 5, 6, 7, 8, 9, 10, 11] and their application to mission-critical structures in the aerospace sector [12].

At the lamina level, the use of *thin-plies* leads to more regular and homogeneous microstructures [6, 9]. Measurements of ply level properties (tensile and compressive modulus, Poisson's ratio, ultimate tensile strength,tensile onset of damage, interlaminar shear strength) on UD specimens ($[0^\circ_m]$ and $[90^\circ_m]$)

revealed no remarkable difference with average properties available in the literature for the same type of fiber, nor showed any particular dependence on the ply thickness [9]. Only an increase of the ultimate compressive strength in the fiber direction was observed with very thin plies ($\sim$ 4 fiber diameters), although with very scattered values, which the authors claim to be due to the fiber arrangement's increased regularity which prevents the onset of fiber microbuckling [9]. A number of researchers [2, 3, 4] has reported improvements in fatigue life with the use of *thin-plies*, which are explained as a consequence of delayed propagation of free edge delaminations and intralaminar cracks. Several researchers have analyzed the effect of *thin-plies* on damage development under static [3, 4, 5, 6, 7, 8, 9], fatigue [2, 3, 4, 5, 9] and impact loadings [3, 4, 5, 9]. It seems apparent that *thin-ply* laminates possess an increased ability to delay, and in some cases even suppress, the onset and propagation of intralaminar cracks (called often transverse or matrix or micro-cracks).

The first stage in the appearance of transverse cracks is known to be the occurrence of fiber/matrix interface cracks (also referred to as debonds), which grow along the fiber arc direction, then kink out of the interface and coalesce forming a transverse crack [13]. Different approaches have been applied to model the initiation and growth of debonds. The Cohesive Zone Model (CZM) has been used to mimic the propagation of debonds along fiber interfaces; coupled with a failure criterion for the matrix, it has provided simulations of the growth of transverse cracks starting from a virgin material [14, 15, 16, 17]. The main advantages of this approach are the possibility to observe the development of a simulated crack path and to record a load-displacement curve to compare with experimental measurement. However, various observations cast a doubt about the applicability of the CZM: the bi- (for 2D models) and tri- (in 3D) axiality of the matrix stress state in the inter-fiber region that is linked with a cavitation-like failure of the polymer [18]; the locality and mode dependency of the interface failure [19]; the problematic use at the microscopic level of properties measured in UD specimens at the laminate level [15]. A second approach that obviates these drawbacks is the application of Linear Elastic Fracture Me-

2

chanics (LEFM) arguments to the study of debond growth. The analysis focuses on the evaluation of Mode I and Mode II Energy Release Rate (ERR) at the crack tip by means of the Virtual Crack Closure Technique (VCCT) [20] or the J-Integral method [21]. The stress and strain field, required for the ERR computation, can be solved by application of different methodologies such as analytical solutions [22], the Boundary Element Method (BEM) [23] or the Finite Element Method (FEM) [24]. This approach presents nonetheless some limitations: it describes propagation of the debond and not its initiation; the role of friction in the contact zone is still an open issue; consensus is still lacking on a proper criterion for crack propagation in mixed mode. Finite fracture mechanics [25] is one way to address the initiation problem. Different studies have followed the LEFM approach and analyzed models of one or two fibers in an effectively infinite matrix [26, 27, 28, 29, 30] and of an hexagonal cluster of fibers in an effectively infinite homogenized UD composite [31, 24]. The problem of debond growth along the fiber-matrix interface in a cross-ply laminate has been only addressed very recently in [32, 33], where authors embed a single partially debonded fiber in an effectively infinite homogenized 90° ply bounded by homogenized 0° layers. Thus, the effect of debond-debond interaction and of the relative proximity of a 0°/90° interface on debond ERR in cross-ply laminates is yet to be addressed. The present work is devoted to this problem. Models of Repeating Unit Cells (RUCs) are developed to represent laminates with different degrees of damage in the 90° ply (here only in the form of debonds). The number of fully bonded fibers across the thickness of the 90° ply is varied in order to investigate the effect of the proximity of the 0°/90° interface. The thickness of the bounding 0° layers is also used as a parameter of the study. The stress and strain fields are solved with the Finite Element Method in Abaqus [34] and the debond (crack) is characterized by its Mode I and Mode II ERR calculated with the VCCT.

2. RVE models & FE discretization

2.1. Introduction & nomenclature

In the present work, we investigate debond development under in-plane longitudinal tension in $[0^\circ_{m \cdot k \cdot 2L}, 90^\circ_{k \cdot 2L}, 0^\circ_{m \cdot k \cdot 2L}]$ laminates. The interaction between debonds in the presence of an interface with a stiff layer is studied with the use of different Repeating Unit Cells (RUCs) (see Figures 1 and 2 in Sec. 2.2), in which only the central fiber is partially debonded. Repetition of the composite RUC occurs along the in-plane longitudinal direction (horizontal direction of the RUC in Figures 1 and 2), thus representing a cross-ply laminate with a thin or even ultra-thin 90° ply in the middle.

All the RUCs present regular microstructures with fibers placed according to a square-packing configuration characterized by the repetition of the same one-fiber unit cell of size $2L \times 2L$, where L is a function of the fiber volume fraction V_f and the fiber radius according to

$$L = \frac{R_f}{2}\sqrt{\frac{\pi}{V_f}}. \tag{1}$$

Each fiber in the model has the same radius R_f, equal to 1 μm. This specific value has no physical meaning per se and it has been selected for simplicity. It is useful to observe that, in a linear elastic solution as the one described in the present article, the ERR is proportional to the geometrical dimensions of the model and thus re-evaluation of the ERR for fibers of any size requires just a multiplication. Furthermore, it is worth to point out that V_f is the same in the one-fiber unit and in the overall RUC, i.e. no clustering of fibers is considered. The thickness of the 90° ply depends on the number k of fiber rows present across the thickness (the vertical or z direction in Figures 1 and 2) according to

$$t_{90^\circ} = k \cdot 2L. \tag{2}$$

On the other hand, the thickness of 0° layers can be assigned freely as a multiple of the 90° ply thickness as

4

$$t_{0°} = m \cdot t_{90°} \tag{3}$$

where m is an arbitrary integer. Thus, the thickness ratio m represents one additional parameter for the investigation.

In the following, let us consider in-plane coordinates x and y, where x is the longitudinal direction of the cross-ply laminate under consideration and thus the transverse direction of its central 90° layer. In the presence of a load in the x-direction, the strain in the y-direction is small, due to the very small Poisson's ratio of the laminate. Furthermore, debonds are considered to be significantly longer in the fiber direction than in the arc direction [35]. Therefore we use 2D models under the assumption of plane strain, defined in the $x - z$ section of the composite. The study presented in this paper thus applies to long debonds and its focus is on understanding the mechanisms of growth along their arc direction. The laminates are assumed to be subject to tensile strain, which is applied in the form of a constant displacement in the x-direction along both vertical boundaries of the RUC as shown in Figure 3.

We assume damage to be present only in the central "row" of fibers of the 90° layer in the form of multiple debonds appearing at different regular intervals along the loading (horizontal) direction. The number of fibers n present in the horizontal direction of the RUC (Figures 1 and 2) controls the distance, in terms of fully bonded fibers, between consecutive debonds: if the RUC has n fibers in the horizontal direction, two consecutive debonds are separated by $n - 1$ undamaged fibers. The RUCs considered are thus Representative Volume Elements (RVEs) of cross-ply laminates with a certain distribution of debonds in the middle 90° layer.

In summary, the models are differentiated by: first, the spacing between debonds along the horizontal direction in the 90° layer, which corresponds to the number n of fibers in the RUC's horizontal direction; second, the thickness of the middle 90° ply measured in terms of the number k of fiber rows in the vertical direction; third, the factor m which provides the thickness of 0° layers as a multiple of

the 90° ply thickness. It thus seems natural to introduce a common notation for the RUCs as $n \times k - m \cdot t_{90°}$.

An additional family of RUCs is considered to study the effect of equivalent boundary conditions, which is constituted by only one partially debonded fiber. Homogenized 0° layers are not present. The application of coupling of horizontal displacements u_x along the right and left sides allows for repetition along the horizontal direction. When the upper boundary of the RUC is left free, we define the $1 \times 1 - free$ model. If coupling of the vertical displacements u_z is applied to the upper boundary, we define instead the $1 \times 1 - coupling$ model. In the case a linear distribution of the horizontal displacement u_x is applied to the upper boundary, the model is refered to as $1 \times 1 - H$. Finally, when the linear distribution of the horizontal displacement u_x is superimposed to the condition of coupling of the vertical displacements u_z on the upper boundary, we have the $1 \times 1 - coupling + H$. Further details about this family of RUCs and the corresponding laminate RVE can be found in [36].

2.2. Description of modelled Representative Volume Elements (RVEs)

The first family of Representative Volume Elements (RVEs) is represented in Figure 1. It represents a set of $[0°_{m \cdot k \cdot 2L}, 90°_{k \cdot 2L}, 0°_{m \cdot k \cdot 2L}]$ laminates with an ultra-thin 90° layer, constituted by a single row of fibers across the thickness. Debonds appear at regular intervals measured in terms of number $n - 1$ of fully bonded fibers present between them, which in turn correspond to the number of fibers along the horizontal direction of the RVE as highlighted in Fig. 1. They are thus the $n \times 1 - m \cdot t_{90°}$ models, where $m = 1, 10$ and n is an integer ≥ 1 ($n = 1$ corresponds to the case of a debond appearing on all the fibers in the central 90° layer). These models are geometrically extreme, but allow to focus on the interaction between debonds and the inter-ply 0°/90° interface. Furthermore, the *spread tow* technology is today capable of producing cross-ply laminates with the central 90° layer thickness only $4-5$ times the fiber diameter, as shown for example in [6], which may in future give practical relevance even to such extreme case.
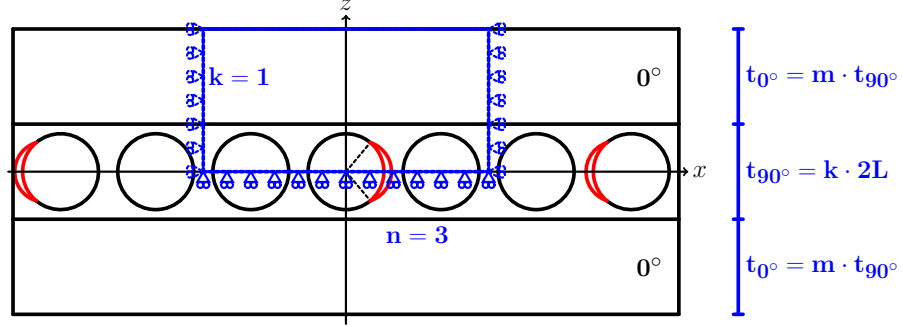
6

Figure 1: Models of $\left[0^\circ_{m \cdot k \cdot 2L}, 90^\circ_{k \cdot 2L}, 0^\circ_{m \cdot k \cdot 2L}\right]$ laminates with an ultra-thin 90° layer, where the 90° ply is made up by a single "row" of fibers. Debonds are repeating at different distances, measured in terms of the number $n-1$ of fully bonded fibers appearing between two consecutive debonds. $2L$ is the thickness of one-fiber row.

The second set of models considers instead cross-ply laminates with a central 90° ply of variable thickness, measured in terms of number k of fiber rows "stacked" in the vertical direction in Figure 2. Once again, debonds appear in

155   the central row only at regular intervals measured in terms of number $n - 1$ of fully bonded fibers present between them, as highlighted in Fig. 2. These models are thus the $n \times k - m \cdot t_{90^\circ}$ models, where $m = 1, 10$, $k > 1$ and n is an integer ≥ 1 ($n = 1$ corresponds to the case of a debond appearing on all fibers of the central fiber row in the 90° layer).

160   By increasing the number n of fibers in the horizontal direction in the RUC, decreasing levels of damage (debonds spaced further apart and the interaction between debonds becomes less important) are considered to be present in the laminate. By increasing the number k of fiber rows, the thickness of the 90° layer is increased and the effect of the relative proximity of the inter-ply $0^\circ/90^\circ$

165   interface can thus be studied. Finally, by increasing the factor m, the thickness of the 0° layers is increased for a given thickness of the 90°, which allows the investigation of the 0° ply-block effect [37].

7
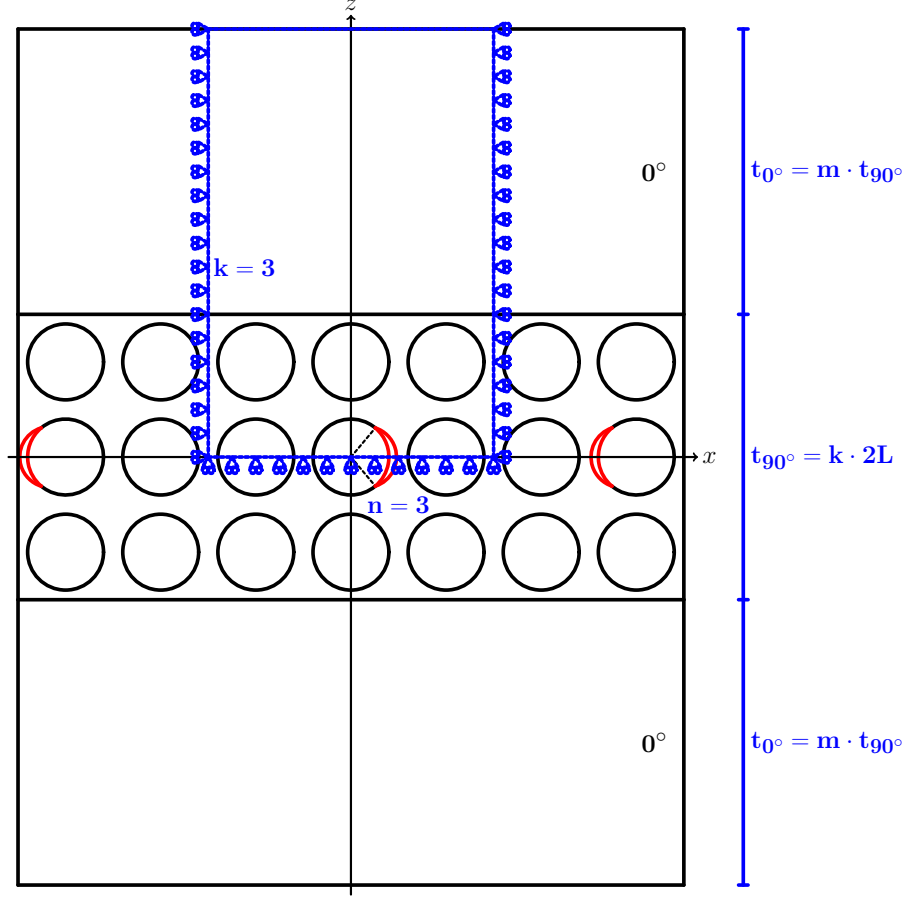
Figure 2: Models of $\left[0^\circ_{m \cdot k \cdot 2L}, 90^\circ_{k \cdot 2L}, 0^\circ_{m \cdot k \cdot 2L}\right]$ laminates with a 90° layer of variable thickness, determined by the number k of "rows" of fibers along the vertical direction. Debonds are repeating at different distances along the horizontal direction, measured in terms of the number $n-1$ of fully bonded fibers appearing between two consecutive debonds. $2L$ is the thickness of one-fiber row.

2.3. Finite Element (FE) discretization

The RUCs are discretized and solved with the Finite Element Method (FEM) using the commercial FEM package Abaqus [34]. The total length and height of a RUC are determined by the number of fibers n in the horizontal direction, the number of fiber rows k across the thickness and the thickness ratio m (see Sec. 2.1 and Sec. 2.2).
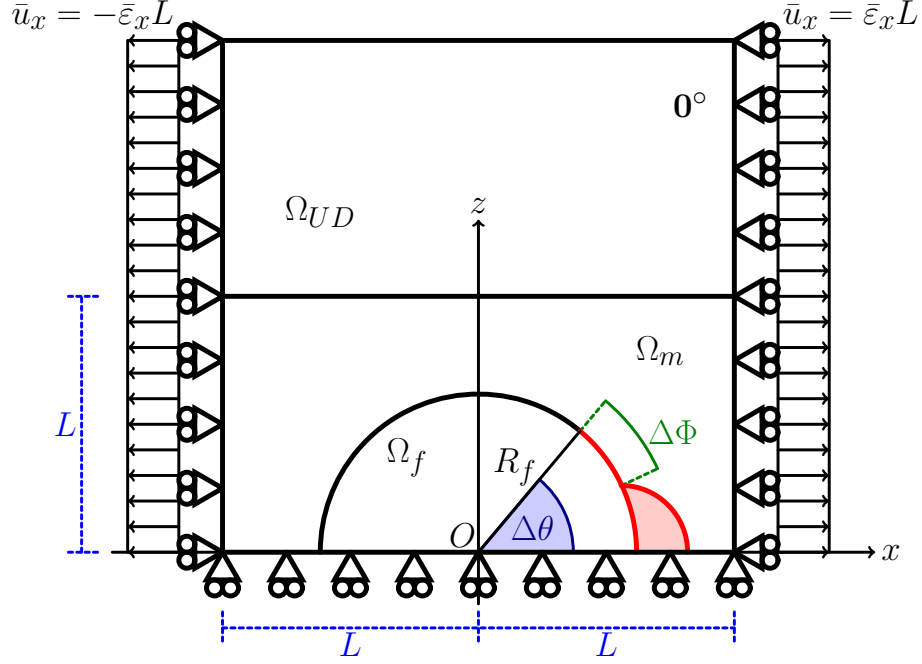
Figure 3: Schematic of the model with its main parameters.

The debond appears symmetrically with respect to the x axis (see Fig. 3)
and we characterize it with the angular size $\Delta\theta$ (the full debond size is thus
$2\Delta\theta$). In the case of large debond sizes ($\geq 60° - 80°$), a region of size $\Delta\Phi$ to be
determined by the solution itself appears at the crack tip. In this region, called
the *contact zone*, the crack faces are in contact and slide on each other. Due
to existence of the contact zone, frictionless contact is considered between the
two crack faces to avoid interpenetration and allow free sliding. Symmetry with
respect to the x axis is applied on the lower boundary. Kinematic coupling on
the x-displacement is applied along the left and right boundaries of the model in
the form of a constant x-displacement $\pm\bar{\varepsilon}_x l$, corresponding to transverse strain
$\bar{\varepsilon}_x$ equal to 1%.

The FEM model is discretized using second order, 2D, plane strain triangular
(CPE6) and rectangular (CPE8) elements. In the crack tip neighborhood, a
refined regular mesh of quadrilateral elements with almost unitary aspect ratio

9

Table 1: Summary of mechanical properties of fiber, matrix and UD layer.

Material	$V_f\,[\%]$	$E_L\,[GPa]$	$E_T\,[GPa]$	$G_{LT}\,[GPa]$	$\nu_{LT}\,[-]$	$\nu_{TT}\,[-]$
Glass fiber	-	70.0	70.0	29.2	0.2	0.2
Epoxy	-	3.5	3.5	1.25	0.4	0.4
UD	60.0	43.442	13.714	4.315	0.273	0.465

is needed to ensure a correct evaluation of the ERR. The angular size δ of an element in this refined region close to the crack tip is by design equal to $0.05°$. The crack faces are modeled as element-based surfaces with a frictionless small-sliding contact pair interaction. The Mode I, Mode II and total Energy Release Rates (ERRs) (respectively G_I, G_{II} and G_{TOT}) represent the main result of the numerical analysis. They are computed using the VCCT [20] implemented in a custom Python routine. Glass fiber and epoxy are considered throughout this article, and it is assumed that their response always lies in the linear elastic domain. The effective UD properties are computed using Hashin's Concentric Cylinder Assembly model [38] with the self-consistency scheme for the out-of-plane shear modulus of Christensen [39]. The properties used are listed in Table 1. The model was validated with respect to BEM results of [40, 29]; considerations about the order of accuracy can be found in [36].

3. Results & Discussion

3.1. Effect of the proximity of the $0°/90°$ interface and of the thickness of the $0°$ layer on debond ERR

We first focus our attention on the model $1 \times 1 - m \cdot t_{90°}$, which represents a particular case of the family $n \times 1 - m \cdot t_{90°}$. It corresponds to a cross-ply laminate in which the central $90°$ ply is constituted by only one fiber row, in which each fiber possesses a debond appearing on alternating sides. The model thus represents an extreme idealization, in the sense that: first, the central $90°$ layer is the thinniest that can be conceived, which allows us to

investigate the direct effect of the proximity of the $0°/90°$ interface on debond ERR; second, a very particular damage state is present for which every fiber is partially debonded from the sorrounding matrix, corresponding to the most severe damage state that can occur in the $90°$ ply when considering debonds as the only mechanism of damage. We are thus focusing on the presence of the $0°/90°$ interface and on the thickness of the $0°$ layer, by considering the ratio $m = \frac{t_{0°}}{t_{90°}}$ of ply thicknessess as a free parameter.
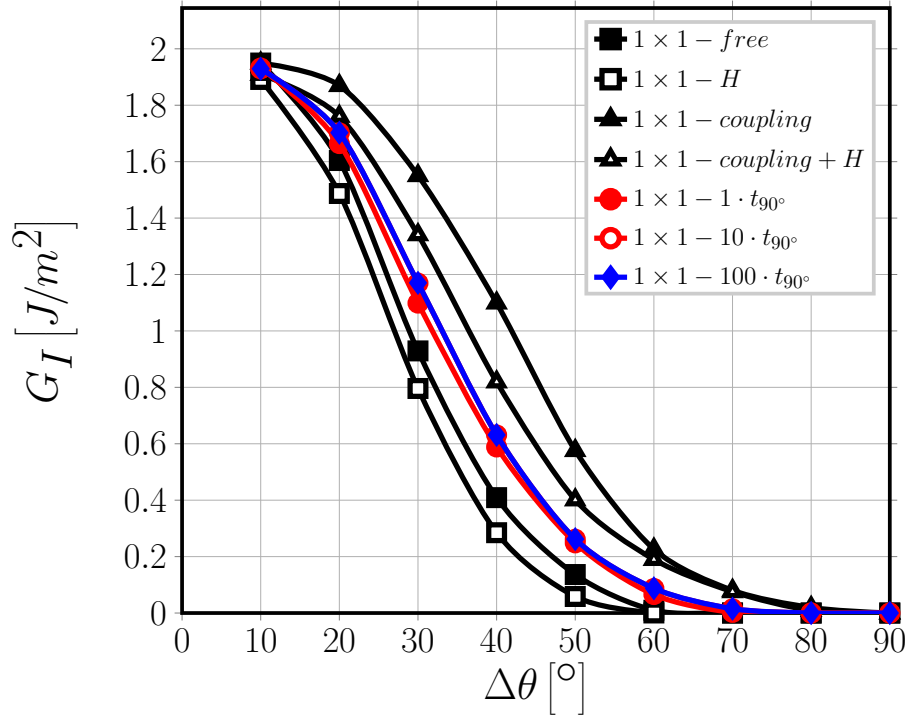

Figure 4: Effect of the proximity of the $0°/90°$ interface and of the thickness of the $0°$ layer on Mode I ERR: models $1 \times 1 - free$, $1 \times 1 - H$, $1 \times 1 - coupling$, $1 \times 1 - coupling + H$ and $1 \times 1 - m \cdot t_{90°}$. $V_f = 60\%$, $\varepsilon_x = 1\%$.

In Figures 4 and 5 it is possible to observe respectively the Mode I and Mode II ERR for models $1 \times 1 - m \cdot t_{90°}$ with $m = 1, 10, 100$. Mode I ERR is practically unaffected by the $0°$ layer thickness, only a marginal increase $\leq 1\%$ can be seen when m is increased from 1 to 10. No further observable change is present when

11

m is increased to 100. Moreover, the contact zone onset, which corresponds to the first value of $\Delta\theta$ such that $G_I = 0$, is always equal to 70° irrespective of the value of m. A more remarkable, albeit small, effect of the 0° layer thickness can be observed for Mode II when m is increased from 1 to values ≥ 10. For open cracks, i.e. when no contact zone is present and thus $\Delta\theta$ is smaller than 70°, increasing the 0° layer thickness causes a reduction of Mode II ERR; while for closed cracks, when a contact zone is present and $\Delta\theta > 70°$, the increase in thickness leads to an increase in ERR.

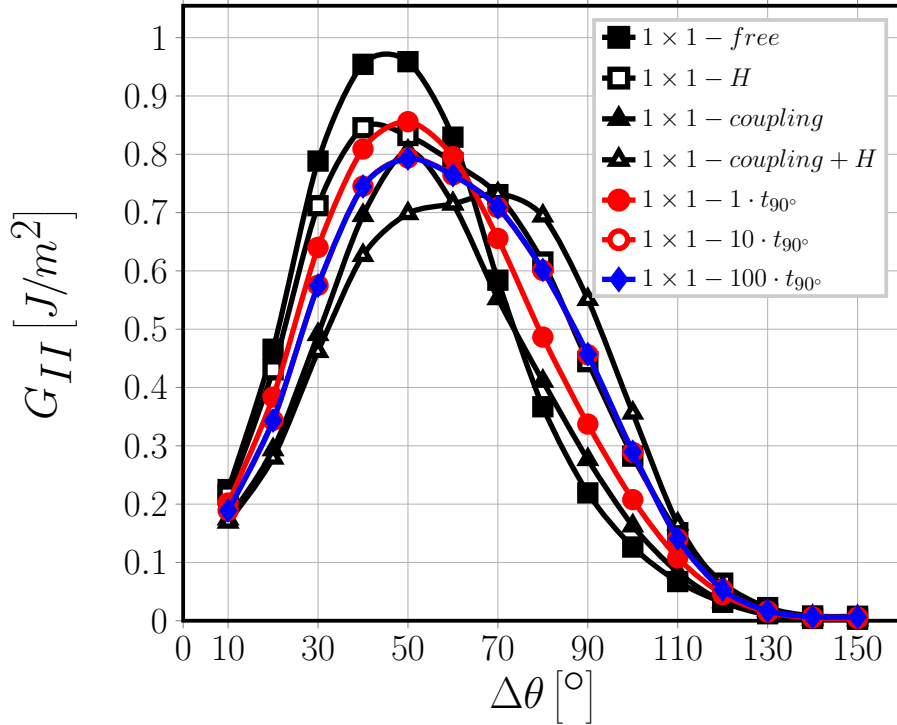Figure 5: Effect of the proximity of the 0°/90° interface and of the thickness of the 0° layer on Mode II ERR: models $1 \times 1 - free$, $1 \times 1 - H$, $1 \times 1 - coupling$, $1 \times 1 - coupling + H$ and $1 \times 1 - m \cdot t_{90°}$. $V_f = 60\%$, $\varepsilon_x = 1\%$.

In order to understand the interaction mechanism between the 0°/90° interface and the debond, Mode I and Mode II ERR are reported respectively in Figures 4 and 5 for models $1 \times 1 - free$, $1 \times 1 - H$, $1 \times 1 - coupling$ and

12

$1 \times 1 - coupling + H$. These RUCs all present equivalent boundary conditions and it is here useful to recall their characteristics: in model $1 \times 1 - free$ the upper bounday is left free; coupling conditions on the vertical displacements u_z are applied to the upper boundary in model $1 \times 1 - coupling$; in model $1 \times 1 - H$ a linearly distributed horizontal displacement u_x is applied to the upper boundary; in model $1 \times 1 - coupling + H$ coupling conditions on the vertical displacements u_z and a linearly distributed horizontal displacement u_x are imposed together on the upper boundary.

Observing Figure 4, it is possible to notice that the values of G_I for the $1 \times 1 - free$ and the $1 \times 1 - coupling$ models represent respectively a lower and an upper bound for the $1 \times 1 - m \cdot t_{90°}$ RVEs: this is true with respect to the value of G_I as well as of contact zone onset (60° for $1 \times 1 - free$, 70° for $1 \times 1 - m \cdot t_{90°}$, 80° for $1 \times 1 - coupling$). When a linearly distributed horizontal displacement u_x is applied to the upper boundary, providing the $1 \times 1 - H$ and $1 \times 1 - coupling + H$ models from the $1 \times 1 - free$ and the $1 \times 1 - coupling$ models, G_I decreases with respect to the "parent" models while the value of $\Delta\theta$ at contact zone onset remains unchanged (60° for $1 \times 1 - free$ and $1 \times 1 - H$, 80° for $1 \times 1 - coupling$ and $1 \times 1 - coupling + H$). Moreover, it is possible to observe that the values of G_I of $1 \times 1 - coupling + H$ are much closer to but always greater than those of $1 \times 1 - m \cdot t_{90°}$ RVEs, thus constituting a more representative upper bound for the latter.

Analogous considerations can be drawn with regard to Mode II (see Fig. 5). For small debonds, $\Delta\theta \leq 30°$, no significant difference in G_{II} can be seen between $1 \times 1 - free$ and $1 \times 1 - H$ and between $1 \times 1 - coupling$ and $1 \times 1 - coupling + H$. With respect to $1 \times 1 - m \cdot t_{90°}$ RVEs, the first pair ($1 \times 1 - free$ and $1 \times 1 - H$) represents the lower bound while the second pair ($1 \times 1 - coupling$ and $1 \times 1 - coupling + H$) the upper bound. For $30° < \Delta\theta \leq 60°$, $1 \times 1 - H$ and $1 \times 1 - coupling + H$ provide significantly lower values of G_{II} than respectively $1 \times 1 - free$ and $1 \times 1 - coupling$. G_{II} values of $1 \times 1 - H$ are very close to $1 \times 1 - 1 \cdot t_{90°}$, even coincident for $\Delta\theta = 60°$. On the other hand, G_{II} values of $1 \times 1 - coupling$ are very close to $1 \times 1 - m \cdot t_{90°}$ with $m \geq 10$ and even coincident

13

for $\Delta\theta = 50°$. For $60° < \Delta\theta \leq 110°$, the situation changes. $1 \times 1 - free$ and $1 \times 1 - coupling$ provides values of G_{II} close to each other, even coincident for $\Delta\theta = 70°$. values of G_{II} of $1 \times 1 - H$ and $1 \times 1 - coupling + H$ are significantly larger than both $1 \times 1 - free$ and $1 \times 1 - coupling$. Furthermore, G_{II} values of $1 \times 1 - H$ coincide with those of $1 \times 1 - m \cdot t_{90°}$ with $m \geq 10$. Mode II ERR of $1 \times 1 - 1 \cdot t_{90°}$ is instead close, but not coincident, to that of $1 \times 1 - coupling$. For $\Delta\theta > 110°$, G_{II} is the same for all models and reaches 0 at a debond size of around 130°, showing that no further growth is possible for such large debonds. These results help to understand the effect of the $0°/90°$ interface on debond ERR. The presence of the stiff homogenized $0°$ layer causes the matrix placed relatively far from the fiber (close to the interface) to contract much less than it would do in the presence of a free surface due to its relatively high Poisson's ratio. Furthermore, the presence of the $0°/90°$ interface induces a more homogeneous x-displacement field all over the matrix domain.

For small debonds ($\Delta\theta < 60° - 70°$), it causes a concurrent increase of G_I and decrease of G_{II}. For small debonds in fact, the Crack Opening Displacement at the crack tip

$$COD \sim \cos(\Delta\theta)u_x + \sin(\Delta\theta)u_z, \tag{4}$$

which governs Mode I according to

$$G_I = \lim_{\Delta a \to 0} \frac{1}{a} \int_a^{\Delta a} \sigma_I(\xi) \, COD(\xi) \, d\xi, \tag{5}$$

is mostly due to the global x-displacement field:

$$COD \sim \underset{\sim\, 1 \text{ for } \Delta\theta \to 0}{\underline{\cos(\Delta\theta)}} u_x + \underset{\sim\, 0 \text{ for } \Delta\theta \to 0}{\underline{\sin(\Delta\theta)}} u_z, \tag{6}$$

which increases in the presence of the $0°/90°$ interface. The Crack Sliding Displacement at the crack tip

$$CSD \sim -\sin(\Delta\theta)u_x + \cos(\Delta\theta)u_z, \tag{7}$$

14

which governs Mode II according to

$$G_{II} = \lim_{\Delta a \to 0} \frac{1}{a} \int_a^{\Delta a} \sigma_{II}(\xi) \, CSD(\xi) \, d\xi, \tag{8}$$

is linked to the global vertical displacement field due to Poisson's effect:

$$CSD \sim \underbrace{-\sin(\Delta\theta)}_{\sim\, 0 \text{ for } \Delta\theta \to 0} u_x + \underbrace{\cos(\Delta\theta)}_{\sim\, 1 \text{ for } \Delta\theta \to 0} u_z \sim \nu u_x, \tag{9}$$

effect that is lower in the presence of a $0°$ layer instead of a free surface thanks to the stiffness of the former. This causes also the delay in the onset of the contact zone. For large debonds ($\Delta\theta > 60° - 70°$) instead, after the onset of the contact zone, the situation reverses:

$$COD \sim \underbrace{\cos(\Delta\theta)}_{\sim\, 0 \text{ for } \Delta\theta \to 1} u_x + \underbrace{\sin(\Delta\theta)}_{\sim\, 1 \text{ for } \Delta\theta \to 0} u_z \sim \nu u_x < 0, \tag{10}$$

i.e. the faces are in contact, while

$$CSD \sim \underbrace{-\sin(\Delta\theta)}_{\sim\, 1 \text{ for } \Delta\theta \to 0} u_x + \underbrace{\cos(\Delta\theta)}_{\sim\, 0 \text{ for } \Delta\theta \to 0} u_z. \tag{11}$$

Thus, the increase in magnitude of the global x-displacement field leads to an increase in the crack sliding displacement component at the crack tip and thus in Mode II ERR.

The local bending stiffness of the $0°$ ply seems also to be playing a role. In the presence of a free surface, the matrix in the $90°$ ply contracts significantly more than the fibers due to the mismatch in Poisson's ratios, thus leading to a higher overall contraction of the composite in the inter-fibers regions than above the fibers. This results in a very curved surface, which follows roughly the fibers' curvature. For small debonds ($\Delta\theta < 60° - 70°$), this translates into higher values of the vertical displacement field and thus an increase in Mode II ERR. For large debonds ($\Delta\theta > 60° - 70°$), the curvature of the material around

15

the fiber corresponds to lower values of the horizontal displacement and thus a reduction of G_{II}. In the presence of a $0°$ layer, such deformation is prevented by the bending stiffness of the latter: Mode II ERR decreases for small debonds and increases for large ones. However, as a relatively thin $0°$ layer such as the one in $1 \times 1 - 1 \cdot t_{90°}$ possesses a lower bending stiffness and thus matrix deformation is able to locally bend the interface, Mode II ERR presents a profile close to $1 \times 1 - H$ for small debonds (curved surface but more homogeneous x-displacement) and to $1 \times 1 - free$ for large ones (locally curved surface). For thicker $0°$ layers, the increased bending stiffness prevents the curvature of the interface and Mode II ERR becomes closer to $1 \times 1 - coupling$ for small debonds (reduced Poisson's effect) and to $1 \times 1 - H$ for large ones (increased horizontal displacement due to locally straight surface).

3.2. Effect of the proximity of the $0°/90°$ interface and of the thickness of the $0°$ layer on non-interactive debonds in a one-fiber row $90°$ ply

We turn now our attention to models $n \times 1 - m \cdot t_{90°}$, which correspond to a cross-ply laminate in which the central $90°$ ply is constituted by only one fiber row where multiple partially debonded fibers are present, located at a distance of $n - 1$ fully bonded fibers from each other, and debonds appear on alternating sides of consecutive damaged fibers (see Figure 1). This class of models allows to study the effect of the presence of the $0°$ layer and of its thickness on non-interactive debonds. As observed in a previous work [36], the presence of fully bonded fibers between partially debonded ones in the loading has a strong effect on debond ERR and controls the interaction between debonds. When n is increased, both Mode I and Mode II increase: the addition of stiffer elements, in the form of fully bonded fibers, increase the magnitude of the horizontal displacement field u_x at the crack tip and thus causes higher values of ERR (see Equations 4, 5, 7 and 8). When looked from this perspective, i.e. moving from the most to the least severe state of damage, this effect is referred to as "strain magnification" [36]. From the opposite perspective, from the least to most severe damage state, we talk about "crack shielding" [36, 41]: an increasing
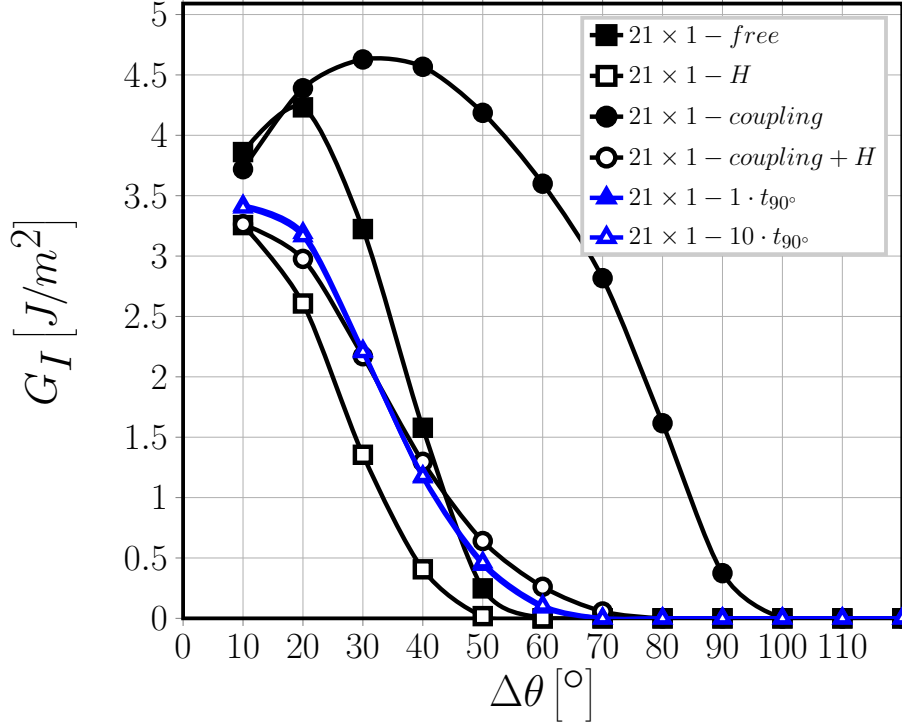
16

Figure 6: Effect of the presence of the 0° layer on Mode I ERR of non-interactive debonds: models $21 \times 1 - free$, $21 \times 1 - H$, $21 \times 1 - coupling$, $21 \times 1 - coupling + H$, $21 \times 1 - 1 \cdot t_{90°}$ and $21 \times 1 - 10 \cdot t_{90°}$. $V_f = 60\%$, $\varepsilon_x = 1\%$.

number of debonds correspond to an increasing number of discontinuities in the horizontal displacement field u_x, which causes a reduction of the magnitude of displacements and strains and thus of ERR. There seems to exist a characteristic 335 distance, measured in terms of fully bonded fibers, above which a change in the number of undamaged fibers affects only marginally, or even not all, debond ERR. This distance, generally $n \sim 20$, marks the transition between a non-interactive solution $(n > 20)$ and an interactive one $(n < 20)$. The "strain magnification" effect thus represents the transition from the interactive to the 340 non-interactive solution, while the "crack shielding" effect the transition from the non-interactive to the interactive solution. If in Sec. 3.1 we studied the effect of the proximity of the 0°/90° interface and of the thickness of the 0° layer on

17

interactive debonds $(1 \times 1 - \dots)$, we analyze in the present section the effect of the $0°/90°$ interface and of the $0°$ layer thickness on non-interactive debonds $(n \times 1 - \dots$ with $n > 20)$.
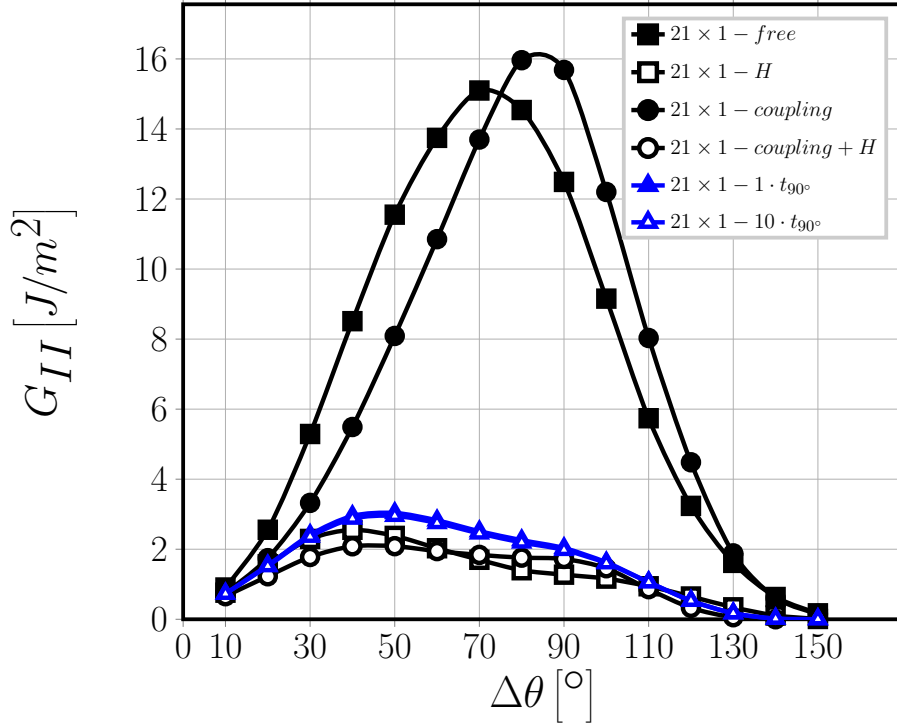

Figure 7: Effect of the presence of the $0°$ layer on Mode II ERR of non-interactive debonds: models $21 \times 1 - free$, $21 \times 1 - H$, $21 \times 1 - coupling$, $21 \times 1 - coupling + H$, $21 \times 1 - 1 \cdot t_{90°}$ and $21 \times 1 - 10 \cdot t_{90°}$. $V_f = 60\%$, $\varepsilon_x = 1\%$.

Comparing Fig. 6 with Fig. 4 and Fig. 7 with Fig. 5, it is possible to observe how increasing the number of fully bonded fibers between consecutive debonds in the loading leads to an increase in Mode I and Mode II ERR. The peak G_I increases from $1.93 \left[\frac{J}{m^2}\right]$ in $1 \times 1 - 1 \cdot t_{90°}$ to $3.42 \left[\frac{J}{m^2}\right]$ in $21 \times 1 - 1 \cdot t_{90°}$, while the peak G_{II} from $0.86 \left[\frac{J}{m^2}\right]$ to $3.04 \left[\frac{J}{m^2}\right]$. The value of $\Delta\theta$ at contact zone onset remains instead the same $(70°)$.

The effect of the $0°$ layer thickness is instead non-existent: values of both G_I and G_{II} are coincident for $21 \times 1 - 1 \cdot t_{90°}$ and $21 \times 1 - 10 \cdot t_{90°}$.

In agreement with the introductory considerations of this section and the results in [36], it is possible to observe in Figures 6 and 7 that $21 \times 1 - free$ and $21 \times 1 - coupling$, in which the horizontal displacement u_x is left uncostrained, show both the highest values of Mode I and Mode II ERR as well as the maximum increase with respect to the interactive case ($1 \times 1 - free$ and $1 \times 1 - coupling$). When a linearly distributed horizontal displacement is applied to the upper boundary, thus constraining the magnitude of the strain magnification effect, both the values of Mode I and Mode II ERR as well as their increase with respect to the interactive case are significantly reduced. Interestingly, $21 \times 1 - coupling + H$ represents, when considering both Mode I and Mode II ERR, the best approximation to the results of $21 \times 1 - m \cdot t_{90°}$ using equivalent boundary conditions. The $0°/90°$ interface, by remaining straight (coupling conditions on the vertical displacements) and controlling the magnitude of the horizontal displacement (applied linearly distributed horizontal displacement), acts against the strain magnification effect and reduces debond ERR. It seems reasonable to conclude that debond growth is favored (i.e. higher ERR) in the presence of strain or stress concentrations (as for example in the presence of a free surface or only coupling conditions on the vertical displacement), while more uniform strain and stress fields as those created by the proximity of the $0°/90°$ interface reduce both Mode I and Mode II ERR and prevent debond growth.

3.3. Effect of the presence of fiber rows with no damage on the debond-$0°/90°$ interface interaction

After having investigated the effect of the proximity of the $0°/90°$ interface and of the thickness of the $0°$ layer on debond ERR for different cases of debond-debond interaction in the same fiber row, we address in this section the effect of the presence of fiber rows with only fully bonded fibers on the interaction between debonds and the $0°/90°$ interface. In other words, we are separating the debond from the $0°/90°$ interface by inserting rows of fully bonded fibers in between, thus increasing the distance to the interface. We consider only the case $m = 1$, i.e. $t_{0°} = t_{90°}$, given that increasing the $0°$ layer thickness does not

19

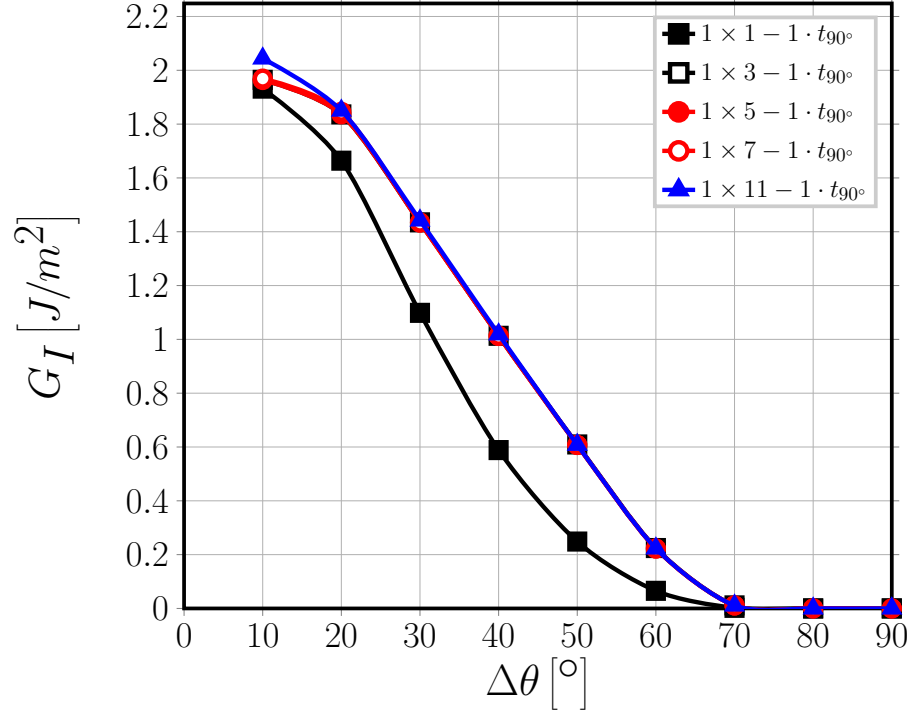Figure 8: Effect of the presence of undamaged fiber rows in the 90° layer on debond-0°/90° interface interaction for Mode I ERR: models $1 \times k - free$ and $1 \times k - 1 \cdot t_{90°}$. $V_f = 60\%$, $\varepsilon_x = 1\%$.

result in any remarkable effect on ERR as shown in Sec. 3.1 and Sec. 3.2.

385   Following the same philosophy of Sec. 3.1 and Sec. 3.2, we analyze the effect of the presence of fiber rows with no damage on debond ERR: first, when the central fiber row possesses only partially debonded fibers, representing the most severe damage state for these RUCs and the solution for interactive debonds (models $1 \times k - 1 \cdot t_{90°}$ in Figures 8 and 9); afterwards, the case of debonds

390 separated by fully bonded fibers in the central fiber row, corresponding to the least severe state of damage and to the solution for non-interactive debonds (models $21 \times k - 1 \cdot t_{90°}$ in Figures 10 and 11).

    Observation of Fig. 8, Fig. 9, Fig. 10 and Fig. 11 reveals that no difference can be seen in Mode I and Mode II ERR by increasing the number k of rows with
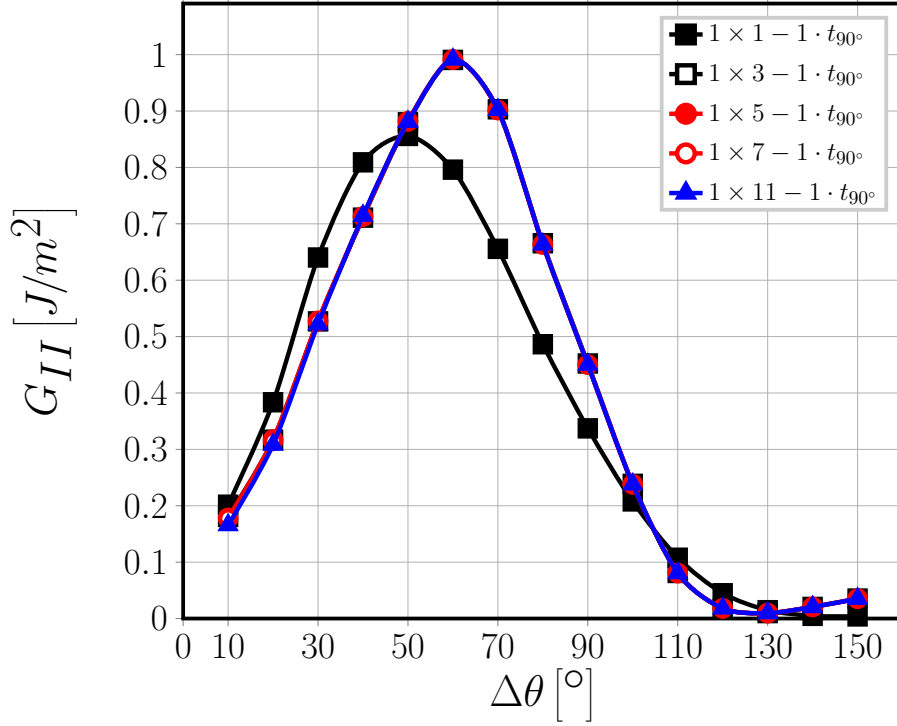
Figure 9: Effect of the presence of undamaged fiber rows in the 90° layer on debond-0°/90° interface interaction for Mode II ERR: models $1 \times k - free$ and $1 \times k - 1 \cdot t_{90°}$. $V_f = 60\%$, $\varepsilon_x = 1\%$.

undamaged fibers when $k \geq 3$, which means that debond ERR does not change once at least 1 row of undamaged fibers is present between the debond and the 0°/90° interface. A significant change is visible only when $k = 1$, which means that no row of fibers with no damage is present between the debond and the 0°/90° interface. This change, from $k \geq 3$ to $k = 1$, is in particular a reduction of both G_I and G_{II}. The results of Figures 8, 9, 10 and 11 imply that the mechanisms of debond-0°/90° interface interaction described in Sec. 3.1 and Sec. 3.2 are actually very localized and that debond ERR is affected by the presence of the 0°/90° interface only when no fully bonded fiber is placed in between. Given that the number k of fibers in the RUC vertical direction corresponds to the thickness of the 90° ply measured in terms of rows of fibers present through
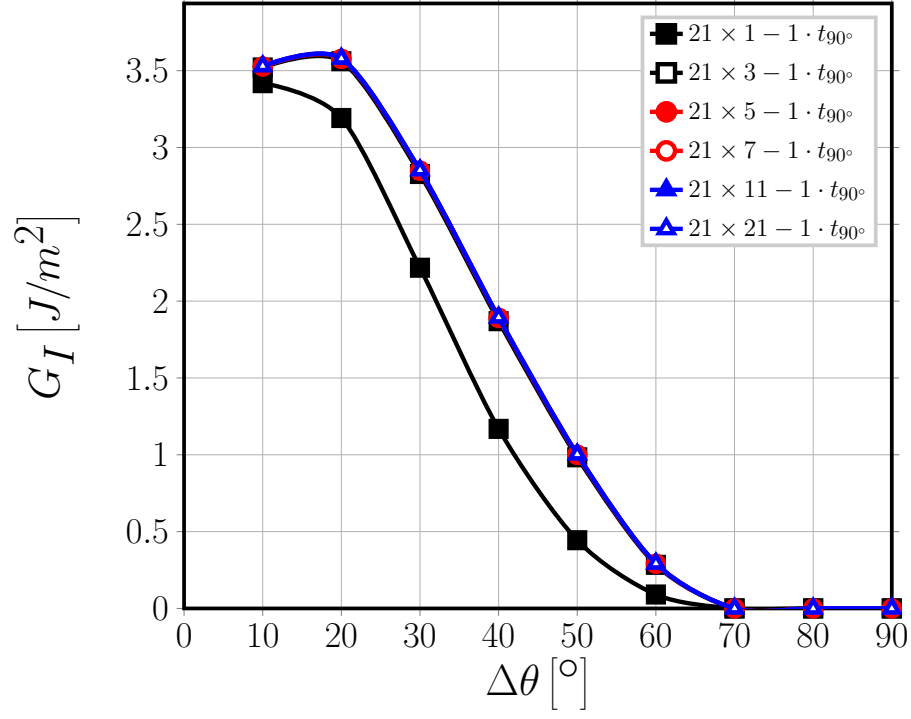
Figure 10: Effect of the presence of undamaged fiber rows in the 90° layer on debond-0°/90° interface interaction for Mode I ERR: models $n \times k - free$ and $n \times k - 1 \cdot t_{90°}$. $V_f = 60\%$, $\varepsilon_x = 1\%$.

its thickness, the results here presented point to another conclusion: the ply-thickness effect does not seem to apply to debond growth, unless an *ultra-thin* ply constituted by only one fiber row ($k = 1$) is considered.

Analogous results can be found in [32, 33], where the authors investigate the ply-thickness effect on debond growth using: first, a single centrally-placed partially debonded fiber with surrounding matrix corresponding to $V_f = 55\%$, embedded from all sides in a homogenized 90° ply bounded by homogenized 0° layers; second, one partially debonded fiber placed in the center and a second partially debonded fiber placed at an angle θ_2 with respect to the horizontal direction with surrounding matrix corresponding to $V_f = 55\%$, embedded from all sides in a homogenized 90° ply bounded by homogenized 0° layers. The thickness
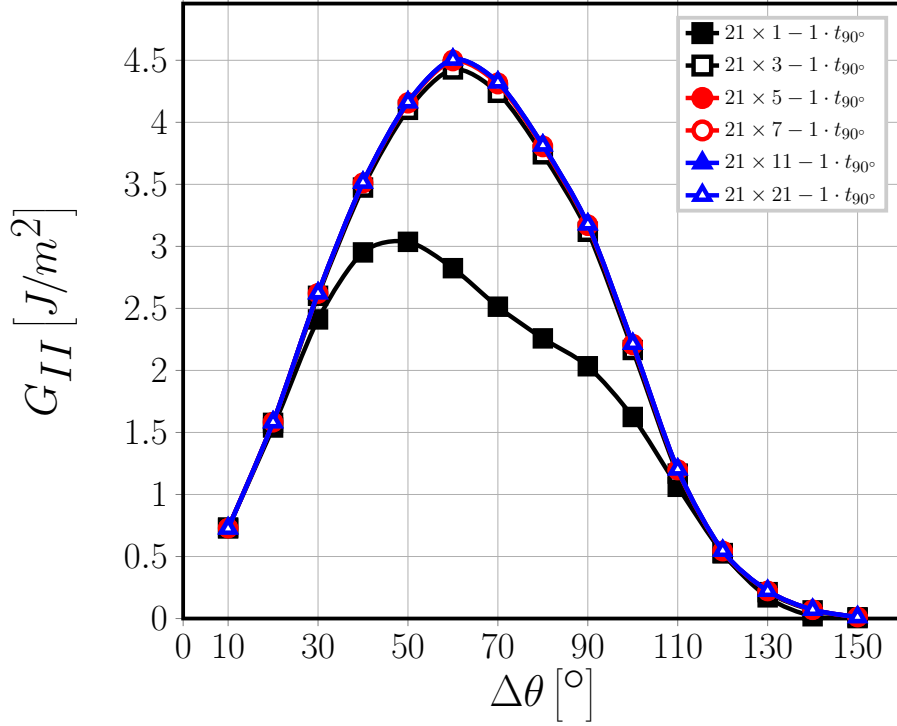
22

Figure 11: Effect of the presence of undamaged fiber rows in the 90° layer on debond-0°/90° interface interaction for Mode II ERR: models $n \times k - free$ and $n \times k - 1 \cdot t_{90°}$. $V_f = 60\%$, $\varepsilon_x = 1\%$.

of the 0° layer is chosen as reference and a $\left[0_p^\circ, 90_{r \cdot p}^\circ\right]_S$ laminate is considered. Carbon-epoxy and glass-epoxy systems are both studied. The thickness of the 90° ply, $t_{90°} = r \cdot t_{0°}$, varies from $r = 3$ (thick 90° ply, > 100 fiber diameters) to $r = 0.1$ (thin 90° ply, $\sim 4 - 5$ fiber diameters). No measurable ply-thickness effect is observed. Experimental support to the claim that the ply-thickness effect has no influence on debond growth can be also found in the literature, in [6]. The authors conducted *in-situ* observations of edge micro-cracks with an optical microscope on $[0_2^\circ, 90_n^\circ, 0_2^\circ]$ carbon fiber-epoxy laminates with $n = 1, 2, 4$, corresponding to a 90° ply thickness of respectively 40 $[\mu m]$ ($\sim 6 - 8$ fiber diameters), 80 $[\mu m]$ ($\sim 12 - 16$ fiber diameters) and 160 $[\mu m]$ ($\sim 24 - 32$ fiber diameters). For $n = 1$, i.e. the case of a very thin 90° ply, isolated debonds

23

appear at a lower value of the applied strain than in thicker plies (at 0.4% vs 0.7%) while coalescence of debonds is suppressed and no transverse crack can be observed even at a strain of 1.5%. The ply-thickness effect was thus observed in [6] for transverse cracks, i.e. coalescence of debonds was delayed to higher strains and even suppressed, but not for debond growth. The analysis presented in this article brings new arguments to the claim that the ply-thickness effect does not influence the growth of debonds.

4. Conclusions

Different models of Repeating Unit Cell, representing different cross-ply laminates, have been studied in order to study the effect of the presence of the $0°$ layer and of its thickness on debond Energy Release Rate for interactive and non-interactive debonds. In order to investigate the mechanisms of the debond-$0°/90°$ interface interaction, Mode I and Mode II ERR of cross-ply RUCs are compared with those of RUCs with equivalent boundary conditions on the upper boundary: a free boundary; coupling conditions on the vertical displacements; an applied linear distribution of the horizontal displacement; coupling conditions on the vertical displacements superimposed to an applied linear distribution of the horizontal displacement. It has been found that:

– by forcing the $0°/90°$ interface to remain approximately straight and controling the magnitude of the horizontal displacements in the composite (and thus in the $90°$ ply), the presence of the $0°$ layer causes more homogeneous distributions of horizontal and vertical displacements, reducing the ERR at the debond crack tip;

– the thickness of the $0°$ layer does not affect the Energy Release Rate, except for a marginal change when $t_{0°} = t_{90°}$ in the case of interactive debonds;

– no difference in ERR is seen when one or more rows of fibers with no damage are present between the debond and the $0°/90°$ interface, a change

24

is observed only no row of undamaged fibers is present between the debond and the 0°/90° interface;

– no effect of the 90° layer thickness, measured in terms of number k of rows of fibers, is observed when $k \geq 3$, a reduction in ERR takes place only when the thickness is reduced to only one fiber row ($k = 1$).

The results reported in this article strengthen the claim that the ply-thickness effect does not influence the growth of debonds, as previously suggested in the literature [6, 17, 32, 33].

Acknowledgements

References

[1] K. Kawabe, New spreading technology for carbon fiber tow and its application to composite materials, Sen'i Gakkaishi 64 (8) (2008) 262–267. doi:10.2115/fiber.64.p_262.

[2] K. Yamaguchi, H. Hahn, The improved ply cracking resistance of thin-ply laminates, in: Proceedings of the 15th International Conference on Composite Materials (ICCM-15), SAMPE, 2005.

[3] S. Sihn, R. Kim, K. Kawabe, S. Tsai, Experimental studies of thin-ply laminated composites, Composites Science and Technology 67 (6) (2007) 996–1008. doi:10.1016/j.compscitech.2006.06.008.

[4] T. Yokozeki, Y. Aoki, T. Ogasawara, Experimental characterization of strength and damage resistance properties of thin-ply carbon fiber/toughened epoxy laminates, Composite Structures 82 (3) (2008) 382–389. doi:10.1016/j.compstruct.2007.01.015.

[5] T. Yokozeki, A. Kuroda, A. Yoshimura, T. Ogasawara, T. Aoki, Damage characterization in thin-ply composite laminates under out-of-plane transverse loadings, Composite Structures 93 (1) (2010) 49–57. `doi: 10.1016/j.compstruct.2010.06.016`.

[6] H. Saito, H. Takeuchi, I. Kimpara, Experimental evaluation of the damage growth restraining in 90 layer of thin-ply cfrp cross-ply laminates, Advanced Composite Materials 21 (1) (2012) 57–66. `doi:10.1163/ 156855112X629522`.

[7] A. Arteiro, G. Catalanotti, J. Xavier, P. Camanho, Notched response of non-crimp fabric thin-ply laminates, Composites Science and Technology 79 (2013) 97–114. `doi:10.1016/j.compscitech.2013.02.001`.

[8] A. Arteiro, G. Catalanotti, J. Xavier, P. Camanho, Large damage capability of non-crimp fabric thin-ply laminates, Composites Part A: Applied Science and Manufacturing 63 (2014) 110–122. `doi:10.1016/j.compositesa. 2014.04.002`.

[9] R. Amacher, J. Cugnoni, J. Botsis, L. Sorensen, W. Smith, C. Dransfeld, Thin ply composites: Experimental characterization and modeling of size-effects, Composites Science and Technology 101 (2014) 121–132. `doi:10. 1016/j.compscitech.2014.06.027`.

[10] G. Guillamet, A. Turon, J. Costa, J. Renart, P. Linde, J. Mayugo, Damage occurrence at edges of non-crimp-fabric thin-ply laminates under off-axis uniaxial loading, Composites Science and Technology 98 (2014) 44–50. `doi: 10.1016/j.compscitech.2014.04.014`.

[11] J. Cugnoni, R. Amacher, S. Kohler, J. Brunner, E. Kramer, C. Dransfeld, W. Smith, K. Scobbie, L. Sorensen, J. Botsis, Towards aerospace grade thin-ply composites: Effect of ply thickness, fibre, matrix and interlayer toughening on strength and damage tolerance, Composites Science and Technology 168 (2018) 467–477. `doi:10.1016/j.compscitech.2018.08. 037`.

26

[12] A. Kopp, S. Stappert, D. Mattsson, K. Olofsson, E. Marklund, G. Kurth, E. Mooij, E. Roorda, The aurora space launcher concept, CEAS Space Journal 10 (2) (2017) 167–187. `doi:10.1007/s12567-017-0184-2`.

[13] J. E. Bailey, A. Parvizi, On fibre debonding effects and the mechanism of transverse-ply failure in cross-ply laminates of glass fibre/thermoset composites, Journal of Materials Science 16 (3) (1981) 649–659. `doi:10.1007/bf02402782`.

[14] V. Kushch, S. Shmegera, P. Brøndsted, L. Mishnaevsky, Numerical simulation of progressive debonding in fiber reinforced composite under transverse loading, International Journal of Engineering Science 49 (1) (2011) 17–29. `doi:10.1016/j.ijengsci.2010.06.020`.

[15] L. P. Canal, C. González, J. Segurado, J. LLorca, Intraply fracture of fiber-reinforced composites: Microscopic mechanisms and modeling, Composites Science and Technology 72 (11) (2012) 1223–1232. `doi:10.1016/j.compscitech.2012.04.008`.

[16] L. Bouhala, A. Makradi, S. Belouettar, H. Kiefer-Kamal, P. Fréres, Modelling of failure in long fibres reinforced composites by x-FEM and cohesive zone model, Composites Part B: Engineering 55 (2013) 352–361. `doi:10.1016/j.compositesb.2012.12.013`.

[17] M. Herráez, D. Mora, F. Naya, C. S. Lopes, C. González, J. LLorca, Transverse cracking of cross-ply laminates: A computational micromechanics perspective, Composites Science and Technology 110 (2015) 196–204. `doi:10.1016/j.compscitech.2015.02.008`.

[18] L. E. Asp, L. A. Berglund, P. Gudmundson, Effects of a composite-like stress state on the fracture of epoxies, Composites Science and Technology 53 (1) (1995) 27–37. `doi:10.1016/0266-3538(94)00075-1`.

[19] V. Mantič, Interface crack onset at a circular cylindrical inclusion under a remote transverse tension. application of a coupled stress and energy

criterion, International Journal of Solids and Structures 46 (6) (2009) 1287–

₅₄₀   1304. `doi:10.1016/j.ijsolstr.2008.10.036`.

[20] R. Krueger, Virtual crack closure technique: History, approach, and applications, Applied Mechanics Reviews 57 (2) (2004) 109. `doi:10.1115/1.1595677`.

[21] J. R. Rice, A path independent integral and the approximate analysis of

₅₄₅   strain concentration by notches and cracks, Journal of Applied Mechanics 35 (2) (1968) 379. `doi:10.1115/1.3601206`.

[22] M. Toya, A crack along the interface of a circular inclusion embedded in an infinite solid, Journal of the Mechanics and Physics of Solids 22 (5) (1974) 325–348. `doi:10.1016/0022-5096(74)90002-7`.

₅₅₀   [23] F. París, J. C. Caño, J. Varna, The fiber-matrix interface crack — a numerical analysis using boundary elements, International Journal of Fracture 82 (1) (1996) 11–29. `doi:10.1007/bf00017861`.

[24] L. Zhuang, A. Pupurs, J. Varna, R. Talreja, Z. Ayadi, Effects of inter-fiber spacing on fiber-matrix debond crack growth in unidirectional composites

₅₅₅   under transverse loading, Composites Part A: Applied Science and Manufacturing 109 (2018) 463–471. `doi:10.1016/j.compositesa.2018.03.031`.

[25] M. Muñoz-Reja, L. Távara, V. Mantič, P. Cornetti, Crack onset and propagation at fibre–matrix elastic interfaces under biaxial loading using finite

₅₆₀   fracture mechanics, Composites Part A: Applied Science and Manufacturing 82 (2016) 267–278. `doi:10.1016/j.compositesa.2015.09.023`.

[26] E. Correa, V. Mantič, F. París, Effect of thermal residual stresses on matrix failure under transverse tension at micromechanical level: A numerical and experimental analysis, Composites Science and Technology 71 (5) (2011)

₅₆₅   622–629. `doi:10.1016/j.compscitech.2010.12.027`.

28

[27] E. Correa, F. París, V. Mantič, Effect of the presence of a secondary transverse load on the inter-fibre failure under tension, Engineering Fracture Mechanics 103 (2013) 174–189. `doi:10.1016/j.engfracmech.2013.02.026`.

[28] E. Correa, F. París, V. Mantič, Effect of a secondary transverse load on the inter-fibre failure under compression, Composites Part B: Engineering 65 (2014) 57–68. `doi:10.1016/j.compositesb.2014.01.005`.

[29] C. Sandino, E. Correa, F. París, Numerical analysis of the influence of a nearby fibre on the interface crack growth in composites under transverse tensile load, Engineering Fracture Mechanics 168 (2016) 58–75. `doi:10.1016/j.engfracmech.2016.01.022`.

[30] C. Sandino, E. Correa, F. París, Interface crack growth under transverse compression: nearby fibre effect, in: Proceeding of the 18th European Conference on Composite Materials (ECCM-18), 2018.

[31] J. Varna, L. Q. Zhuang, A. Pupurs, Z. Ayadi, Growth and interaction of debonds in local clusters of fibers in unidirectional composites during transverse loading, Key Engineering Materials 754 (2017) 63–66. `doi:10.4028/www.scientific.net/kem.754.63`.

[32] M. Velasco, E. Graciani, L. Távara, E. Correa, F. París, BEM multiscale modelling involving micromechanical damage in fibrous composites, Engineering Analysis with Boundary Elements 93 (2018) 1–9. `doi:10.1016/j.enganabound.2018.03.012`.

[33] F. París, M. L. Velasco, E. Correa, Micromechanical study on the influence of scale effect in the first stage of damage in composites, Composites Science and Technology 160 (2018) 1–8. `doi:10.1016/j.compscitech.2018.03.004`.

[34] Simulia, Providence, RI, USA, ABAQUS/Standard User's Manual, Version 6.12 (2012).

29

[35] H. Zhang, M. Ericson, J. Varna, L. Berglund, Transverse single-fibre test for interfacial debonding in composites: 1. experimental observations, Composites Part A: Applied Science and Manufacturing 28 (4) (1997) 309–315. `doi:10.1016/s1359-835x(96)00123-6`.

[36] L. Di Stasio, J. Varna, Z. Ayadi, Energy release rate of the fiber/matrix interface crack in UD composites under transverse loading: effect of the fiber volume fraction and of the distance to the free surface and to non-adjacent debonds, Theoretical and Applied Fracture Mechanics (2019) 102251`doi:10.1016/j.tafmec.2019.102251`.

[37] R. Teixeira, S. Pinho, P. Robinson, Thickness-dependence of the translaminar fracture toughness: Experimental study using thin-ply composites, Composites Part A: Applied Science and Manufacturing 90 (2016) 33–44. `doi:10.1016/j.compositesa.2016.05.031`.

[38] Z. Hashin, Analysis of composite materials—a survey, Journal of Applied Mechanics 50 (3) (1983) 481. `doi:10.1115/1.3167081`.

[39] R. Christensen, K. Lo, Solutions for effective shear properties in three phase sphere and cylinder models, Journal of the Mechanics and Physics of Solids 27 (4) (1979) 315–330. `doi:10.1016/0022-5096(79)90032-2`.

[40] F. París, E. Correa, V. Mantič, Kinking of transversal interface cracks between fiber and matrix, Journal of Applied Mechanics 74 (4) (2007) 703. `doi:10.1115/1.2711220`.

[41] I. García, V. Mantič, E. Graciani, Debonding at the fibre–matrix interface under remote transverse tension. one debond or two symmetric debonds?, European Journal of Mechanics - A/Solids 53 (2015) 75–88. `doi:10.1016/j.euromechsol.2015.02.007`.

30